Study on the Noise and Structural Parameters of Radiators for Engineering Vehicles

Jie MENG, Xiaolong ZHANG, Hui FENG, Tianshan WEI, and Shangkun SHI

***Abstract*—To investigate the relationship between the noise generated by radiators in engineering vehicles and their structural parameters, this study designs radiator models with different fin spacing for a tracked off-road vehicle. The Lighthill acoustic analogy method is employed to comparatively analyze the aerodynamic noise characteristics of the sound field at the driver's cabin position for different fin spacings. Additionally, the spectral characteristics and sound quality at four typical positions are analyzed. The results indicate that as fin spacing increases, the overall noise of the radiator decreases, with high-noise regions gradually dispersing evenly from the center toward both sides. The optimal fin spacing is found to be 2 mm, at which the radiator noise ranges from 60.76 to 64.3 dB, the lowest among the four radiator configurations tested. Furthermore, a comprehensive noise index based on psychoacoustic parameters is proposed for quantitative comparison. The radiator with a 2 mm fin spacing exhibits the best performance, achieving a 92.3% improvement over the radiator with the poorest comprehensive noise index. These findings provide a scientific basis for the low-noise design of engineering vehicle radiators.**[1]**

***Index Terms*—Radiator; Numerical simulation; Aerodynamic noise; Lighthill's acoustic analogy**

I. Introduction

In large-scale equipment such as engineering vehicles, the engine cooling system generates substantial noise during heat dissipation, with sound pressure levels reaching up to 90 dB. This high noise level not only poses significant risks to the psychological and physical health of drivers but also potentially compromises driving safety. Consequently, investigating and mitigating the noise produced by engine cooling systems is of paramount importance.

The engine cooling system typically comprises a low-speed axial fan and a radiator. Zeng [1] employed numerical simulations with the SST k-ω turbulence model, drawing inspiration from the bionics of shark dorsal fins, to design a fan blade that suppresses the formation of trailing-edge turbulent vortices, effectively reducing aerodynamic noise. Alessandro [2] developed a low-order sound prediction method to analyze the noise emitted by low-speed fans in automotive engine cooling systems. Their approach utilized a semi-analytical model based on Amiet's airfoil theory, accounting for the influence of blade sweep angles on turbulent impingement noise prediction and the mechanisms of trailing-edge noise generation. Liu [3] introduced a blended tip winglet structure to the top of axial fan blades to mitigate aerodynamic losses and noise caused by tip leakage flow. Their numerical analysis demonstrated that this structure reduced aerodynamic noise while enhancing the static pressure efficiency of the axial fan. Wang [4] utilized numerical methods to investigate the noise reduction effects of four distinct mid-camber line distributions on bio-inspired owl wing airfoil blades. Experimental validation confirmed the optimized fan's aerodynamic performance and noise reduction capabilities, revealing that owl wing-inspired blades effectively diminished the aerodynamic noise produced by centrifugal fans in air conditioning systems. Similarly, Liu [5], inspired by the leading-edge structure of owl wings, designed a novel noise-reducing structure for a multi-blade centrifugal fan. Numerical simulations comparing the original and biomimetic designs showed that the latter significantly reduced airflow impact on the fan's volute tongue and suppressed flow separation. Huang [6] applied Detached Eddy Simulation (DES) and Large Eddy Simulation (LES) methods, finding that LES provided more accurate predictions of broadband vortex noise with lower errors. Dong [7] designed biomimetic fan blades modeled after owl wings, with experimental results indicating that the blade's stripe radius was a critical factor in noise reduction. Luo [8] developed a noise prediction model using Computational Fluid Dynamics (CFD) and vortex sound theory, achieving a prediction error of less than 1.5 dB(A) across various fan and heat exchanger configurations, underscoring the model's potential for wider application. Tang [9] incorporated a sawtooth structure with unequal heights and inclined angles at the blade's trailing edge, conducting parametric modeling and orthogonal experiments to assess the effects of different parameters on airflow and noise. Their findings highlighted improvements in both aerodynamic performance and noise reduction for the optimized fan. However, while most research focuses on fan noise control, studies exploring the relationship between radiator noise and structural parameters remain scarce.

Radiator fins play a pivotal role in noise generation and propagation by influencing airflow distribution and turbulence characteristics. Wojciech [10] examined the impact of orifice plates on pressure fluctuation amplitude in pulsating flow through straight pipes, discovering that smaller orifice sizes reduced pressure pulsations. Xie [11] evaluated the vibration and sound pressure levels of various orifice plate types in an anechoic chamber, demonstrating that stepped orifice plates exhibited the least mechanical energy loss and radiated sound pressure. Wang [12]

Manuscript received January 10, 2025; revised April 5, 2025.

This study was supported by the General Program of Natural Science Research of Shanxi Province (Grant No. 202203021221148).

Jie MENG is an associate professor at the School of Vehicle and Transportation Engineering, Taiyuan University of Science and Technology, Taiyuan 030024, China (e-mail: 2018054@tyust.edu.cn).

Xiaolong ZHANG is a postgraduate from the School of Vehicle and Transportation Engineering, Taiyuan University of Science and Technology, Taiyuan 030024, China (e-mail: 2251850433@qq.com).

Hui FENG is a manager at Guizhou Jonyang Kinetics Co., Ltd, Guizhou 550006, China (e-mail: fenghui@jonyang.com).

Tianshan WEI is a manager at Guizhou Jonyang Kinetics Co., Ltd, Guizhou 550006, China (e-mail: weitianshan@jonyang.com).

Shangkun SHI is a postgraduate from the School of Vehicle and Transportation Engineering, Taiyuan University of Science and Technology, Taiyuan 030024, China (e-mail: s202212210228@stu.tyust.edu.cn).

employed Large Eddy Simulation (LES) to estimate flow fields and analyze how tube type, pitch, external flow direction, speed, and length influenced noise in shell-and-tube heat exchangers, shedding light on fluid-induced noise mechanisms. Bi [13] conducted a signal-to-noise ratio (SNR) analysis of structural variables in plate heat exchangers, identifying chevron angle and plate height as the most significant factors affecting overall performance. Anders Rynell [14] introduced a specialized study to determine the acoustic characteristics of automotive cooling packages, utilizing a shrouded subsonic axial fan positioned between a partitioned anechoic chamber and a reverberation room to achieve distinct separation of upstream and downstream sound fields. Hu [15] developed a multi-physics computational model for radiators, considering the coupling effects between heat dissipation and fan noise. Their optimized system enhanced overall heat dissipation by 8% and reduced fan noise by 4.2 dBA, achieving noise reduction without sacrificing cooling efficiency. Han [16] performed a numerical study on the source distribution, directivity, and spectra of flow-induced noise in natural gas manifolds, using orthogonal experimental design and grey relational analysis to quantify parameter influences on overall sound pressure levels and propose noise reduction strategies. Alessandro [17] assessed the downstream turbulence characteristics of radiators, showing that fins and louvered tubes effectively dissipated vortex structures. Czwielong [18] utilized 3D wind speed measurements and smoke visualization to investigate the acoustic interactions between axial fans and heat exchangers, finding that larger heat exchangers reduced total sound power and low-frequency broadband noise. Amoiridis [19] demonstrated that radiators with fine cooling tubes and dense grids had minimal impact on source localization maps and spectra. Turbulence modeling typically relies on isotropic and homogeneous models, such as the von Kármán or Liepmann models [20]. Although these studies primarily focus on measuring noise from orifice plates and heat exchangers, they often provide only superficial descriptions of phenomena, lacking in-depth exploration of the relationship between structural parameters and aerodynamic noise. Research on the distribution of radiator noise and its sound pressure levels remains limited.

This study employs a numerical simulation system and the Lighthill acoustic analogy method to investigate the effects of radiator fin spacing on fluid noise under various operating conditions, analyzing how noise composition and distribution vary with changes in fin spacing.

II. Numerical Calculation Method

In this study, the SST k-ε turbulence model is employed to perform steady-state computations. The governing equations are as follows:

The continuity equation is:

$$\frac{\partial(\rho u)}{\partial x}+\frac{\partial(\rho v)}{\partial y}+\frac{\partial(\rho w)}{\partial z}=0 \tag{1}$$

The momentum equation is:

$$\nabla\cdot(\rho u u_i)=-\nabla p+\nabla\cdot\tau \tag{2}$$

The k-ε equations are:

$$\frac{\partial}{\partial t}(\rho k)+\frac{\partial}{\partial x_i}(\rho u_i k)=\frac{\partial}{\partial x_j}\left[\left(\mu+\frac{\mu_t}{\sigma_k}\right)\frac{\partial k}{\partial x_j}\right]+G_k-\rho\epsilon \tag{3}$$

$$\begin{aligned}&\frac{\partial}{\partial t}(\rho\epsilon)+\frac{\partial}{\partial x_i}(\rho u_i\epsilon)=\\&\frac{\partial}{\partial x_j}\left[\left(\mu+\frac{\mu_t}{\sigma_\epsilon}\right)\frac{\partial\epsilon}{\partial x_j}\right]+C_{\epsilon1}\frac{G_k\epsilon}{k}-C_{\epsilon2}\rho\frac{\epsilon^2}{k}\end{aligned} \tag{4}$$

where ρ represents the density (kg/m³), u denotes the velocity (m/s), p indicates the pressure (Pa), τ is the viscous stress tensor (Pa). Additionally, k , ϵ ,and G_k correspond to the turbulent kinetic energy, the dissipation rate of turbulent kinetic energy, and the production of turbulent kinetic energy due to the mean velocity gradient (J), respectively. The constants $C_{\epsilon1}$, $C_{\epsilon2}$, σ_k and σ_ϵ are standard parameters of the k-ε model. The turbulent viscosity, μ_t is determined as follows:

$$\mu_t=C_\mu\frac{\rho k^2}{\epsilon} \tag{5}$$

where C_μ is the turbulent viscosity constant.

For transient flow simulations, the steady-state flow field serves as the initial condition. As the transient flow field gradually stabilizes, key flow characteristics are extracted. These characteristics are then utilized as an equivalent sound source for subsequent sound field propagation analysis. To investigate the acoustic properties in depth, the Lighthill acoustic analogy method is applied. This approach integrates the momentum and continuity equations of viscous incompressible flow to derive a wave equation and its corresponding sound source term [21] :

$$\begin{aligned}&\frac{\partial^2\rho'}{\partial t^2}-a_0^2\nabla^2\left(\frac{\partial^2\rho'}{\partial t^2}\right)-a_0^2\nabla^2\rho'=\\&\frac{\partial}{\partial t}\left[\rho_0 u_i\frac{\partial f}{\partial x_i}\delta(f)\right]-\frac{\partial}{\partial x_i}\left[p'\delta_{ij}\frac{\partial f}{\partial x_i}\delta(f)\right]+\frac{\partial^2 T_{ij}}{\partial x_i\partial x_j}\end{aligned} \tag{6}$$

where ρ' represents the density fluctuation (kg/m³), p' denotes the sound pressure (Pa), f is the generalized function, and $\delta(f)$ is the Dirac delta function, with the Lighthill stress tensor T_{ij} playing a critical role in the formulation.

III. Computational Model and Setup

A. Geometric Model

This study investigates the flat fin-type aluminum radiator of a tracked off-road vehicle, with a specific focus on the relationship between the radiator's fin spacing and noise generation. Tracked off-road vehicles are typically engineered for extreme terrains and specialized, high-difficulty tasks, as illustrated in Figure 1(a). Owing to the unique positioning of their power systems, these vehicles feature rear-mounted engines, which improve weight distribution and balance, thereby enhancing traction and stability on rough terrain, as depicted in Figure 1(b).

(a) Tracked off-road vehicle.

(b)Rear-mounted engine.

Fig. 1. Ripsaw EV3-F4 tracked off-road vehicle.

To reduce computational complexity, the model was simplified by excluding the influence of components surrounding the radiator core on overall performance.

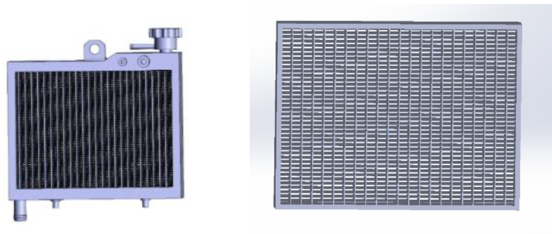

(a) Radiator model. (b) Simplified model.

Fig. 2. Physical model and simplified model of the radiator.

The simplified physical model of the radiator is presented in Figure 1, with detailed structural parameters outlined in Table 1. To explore the impact of fin spacing on noise, four models with fin spacings of 1 mm, 2 mm, 3 mm, and 4 mm were developed for subsequent simulations.

TABLE I

STRUCTURAL PARAMETERS OF THE SIMPLIFIED RADIATOR MODEL

Parameter	Value(mm)
Radiator Length L	240
Radiator Width M	32
Radiator Height H	180
Fin Thickness L_d	0.4
Fin Spacing d	1/2/3/4
Tube Spacing C_p	2
Radiator Length L	240
Radiator Width M	32
Radiator Height H	180

B. Fluent Solving and Acoustic Settings

In this study, the incoming flow velocity was set to 15 m/s. During the initial phase, a pressure-based coupled solver was employed, utilizing the SIMPLE algorithm to compute the steady-state flow field. Subsequently, the solver was switched to the coupled algorithm to simulate the transient flow field and sound field. Once the transient flow field stabilized, flow data from each time step were treated as equivalent sound sources for calculating sound field propagation. The Lighthill volume source [22] was then applied to simulate sound wave propagation from the radiator, and the time-domain signal was transformed into the frequency domain using a discrete Fourier transform. To mitigate high-frequency noise interference, the Hanning window function was applied to smooth the sound signal.

The primary objective of this study is to analyze the noise distribution on the outlet side of the radiator, with particular emphasis on the sound pressure level distribution within the driver's cab sound field. To achieve this, a 1/4 acoustic monitoring sphere [23] was established, centered on the radiator. Monitoring points were positioned every 15° within a 3 m radius on the XOY, ZOY, and ZOX planes, as shown in Figure 3. By analyzing the sound pressure data from these points, the noise distribution in both the near and far fields was examined.

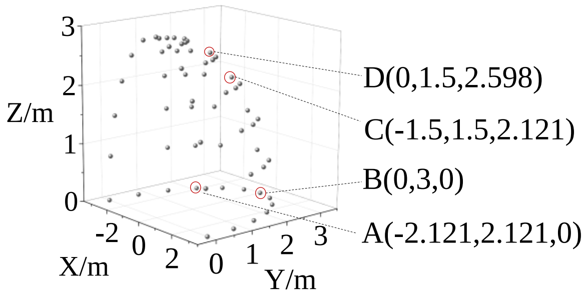

Fig. 3. Monitoring point setup.

Additionally, considering the distance between the radiator and the driver's cab, four representative positions—labeled A, B, C, and D—were selected on the monitoring sphere as monitoring points to capture the sound pressure signal of the radiator noise transmitted to the driver's cab. The specific coordinates of these monitoring points are provided in Table 2, where R denotes the distance from the radiator center to the monitoring point, Θ represents the horizontal angle relative to the positive Y-axis, and Φ indicates the elevation angle relative to the XY plane.

TABLE II

MONITORING POINT LOCATIONS

Spherical coordinates	R(m)	Θ(°)	Φ(°)
A	3	45	0
B	3	0	0
C	3	45	45
D	3	0	60

C. Mesh Independence Verification

A mesh independence test was performed using eight different mesh sizes to ensure that the simulation results were not affected by the mesh resolution. During the test, the pressure drop (ΔP) between the inlet and outlet of the radiator was measured and recorded. The corresponding results for the eight mesh sizes are presented in Table 3, allowing for the assessment of whether further mesh refinement would significantly impact the accuracy of the simulation outcomes.

TABLE III
MESH INDEPENDENCE VERIFICATION

Mesh size(m)	Number of mesh divisions(10^4)	ΔP(Pa)
0.01	27.39	369.91
0.007	53.53	350.25
0.005	113.38	336.43
0.003	345.37	331.96
0.0025	501.65	327.70
0.0023	600.99	326.26
0.002	890.67	327.66
0.0018	1136.47	330.82

The results of the mesh independence verification are presented in Figure 4. It was observed that the pressure drop (ΔP) stabilized as the grid count increased from 530,000 to 1,100,000, with variations remaining within 1% beyond 5,000,000 grids. To balance computational accuracy and efficiency, a grid system consisting of 8,906,718 elements was selected for subsequent simulations.

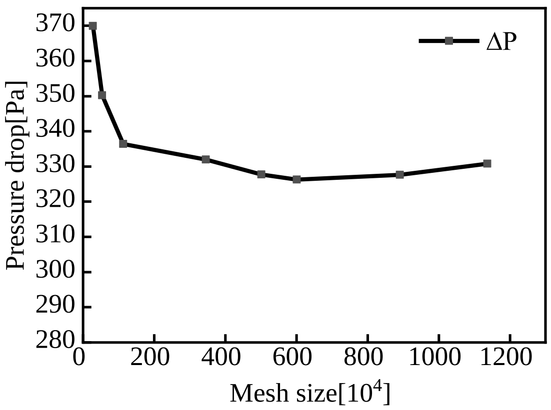

Fig. 4. Results of the mesh independence verification.

IV. FLOW FIELD DISTRIBUTION

Figure 5 illustrates the velocity distribution of the radiator on the y-z plane for different fin spacing conditions.

As gas passes through the radiator, it first experiences rapid compression from the upstream gas, followed by the formation of complex airflows within the channels between the fins. These airflows gradually converge towards the radiator's central region, ultimately developing into turbulence.

A comparison of the velocity distributions across the four cases reveals that the high-speed jet region is smallest in case b and largest in case a. In case a, the gas does not enter the merging zone until the end, indicating the most unstable flow field. In case b, most regions enter the merging zone at z=0.15m, with the overall high-speed jet region being the smallest. Cases c and d exhibit similar lengths and uniform widths in their high-speed jet regions, both entering the merging zone at z=0.35m.

To better interpret these velocity distribution patterns, the dual jet theory can be applied to explain the merging process and assess the flow stability.

The variations in the radiator's fin spacing distribution result in significant velocity differences between the medium flowing through the channels between the fins and the surrounding fluid. This velocity disparity causes the outflowing fluid to mix with the low-speed airflow, entraining the surrounding stationary gas into the main stream. According to dual jet theory [24]-[25], the entrainment effect causes the jets to gradually converge within a certain distance, forming a convergence zone. As the fluid velocity recovers, these jets eventually merge, transitioning into a merging zone, until the core region of the jet becomes indistinct. Thus, by analyzing the size of the merging zone downstream of the radiator, the flow stability can be assessed.

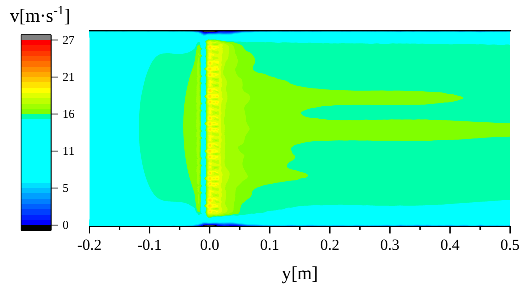

(a) d=1mm.

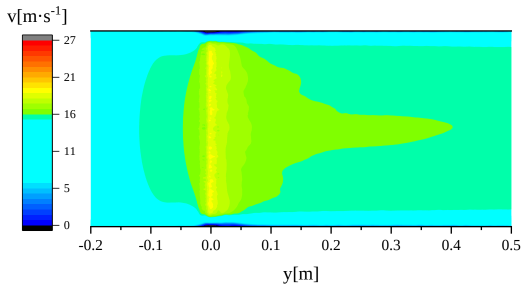

(b) d=2mm.

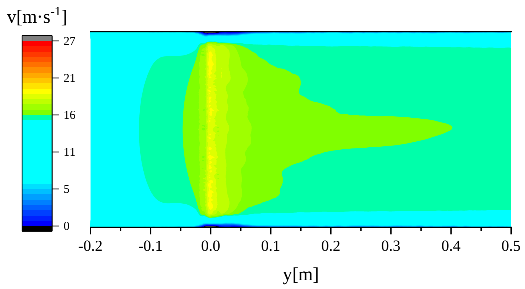

(c) d=3mm.

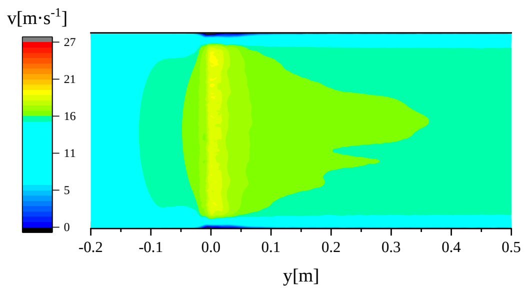

(d) d=4mm.
Fig. 5. Velocity contours of the radiator with different d values.

Therefore, based on the velocity distribution analysis, the radiator with a fin spacing of 2mm (case b) exhibits the smallest high-speed jet region and the most favorable flow characteristics.

V. SOUND FIELD DISTRIBUTION

The flow field characteristics are determined through numerical simulation to analyze the corresponding acoustic field properties. In the simulation of acoustic field propagation, the unsteady flow velocity within the flow field is treated as an equivalent sound source. The Lighthill acoustic analogy equation is utilized to compute the variations in sound pressure from the source region to the monitoring point. Subsequently, a distribution diagram of the total sound pressure level is generated, illustrating the near and far fields of the radiator.

According to references [26]–[27] , the noise sound pressure level is defined as follows:

$$SPL = 10\log\left(\frac{p_{\mathrm{rms}}^2}{p_{\mathrm{ref}}^2}\right) \tag{7}$$

where SPL represents the sound pressure level (dB), p_{rms} denotes the root mean square of the fluctuating pressure (Pa),and p_{ref} is the reference sound pressure, with a value of 20 μPa.

Figure 6 and Table 4 present the relative sound field distribution for radiators with varying fin spacings at an inlet velocity of v = 15 m/s. These visualizations and data tables illustrate how changes in fin spacing significantly influence the overall noise characteristics and the distribution of the sound pressure levels around the radiator.

As observed from the figure, when the fin spacing increases from 1 mm to 4 mm, the overall sound field distribution undergoes a noticeable transformation. Specifically, it evolves from a relatively uniform arch-shaped pattern at smaller fin spacings to a flatter and more irregular configuration as the spacing increases. This change indicates that larger fin spacings result in a more dispersed and less concentrated sound field.

At a fin spacing of 1 mm, the sound field exhibits a significant concentration of noise, with a distinct small high-pressure area located near the central region of the radiator. In this region, the sound pressure level (SPL) ranges from approximately 72 to 73 dB, indicating a relatively intense noise zone. By contrast, the radiator with a 2 mm fin spacing demonstrates a more uniform and widely distributed sound field. The high-pressure area expands considerably, covering a larger portion of the central region. However, the maximum SPL decreases to approximately 63–64 dB, suggesting a more balanced and evenly distributed noise pattern, which is indicative of improved acoustic performance.For radiators with fin spacings of 3 mm and 4 mm, the overall noise levels are slightly elevated compared to the 2 mm spacing. The maximum SPL increases by approximately 3 dB, indicating a modest deterioration in noise performance. This suggests that while larger fin spacings reduce sound field concentration, they also lead to a slight rise in overall noise levels.

In summary, the radiator with a 2 mm fin spacing achieves the best performance in terms of overall noise reduction. Its maximum SPL is approximately 9.16 dB lower than that of the 1 mm spacing, highlighting its superior noise characteristics. These findings regarding the effect of fin spacing on noise closely align with the flow field analysis predictions, confirming the correlation between flow stability and acoustic performance.

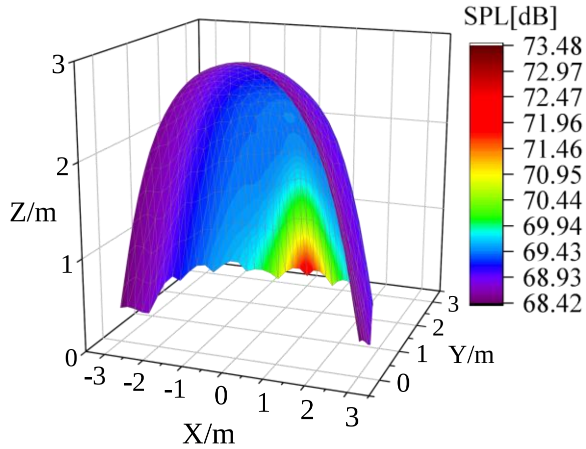

(a) d=1mm.

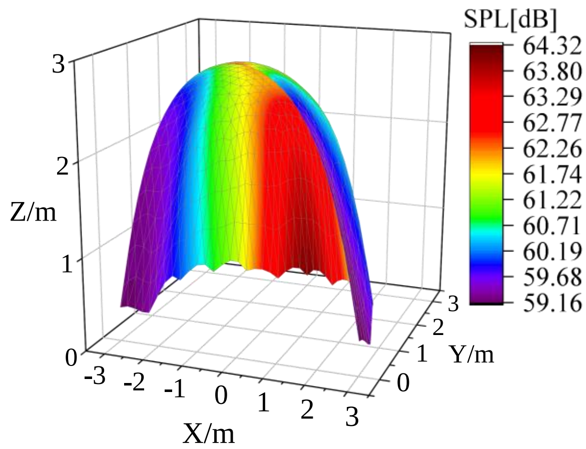

(b) d=2mm.

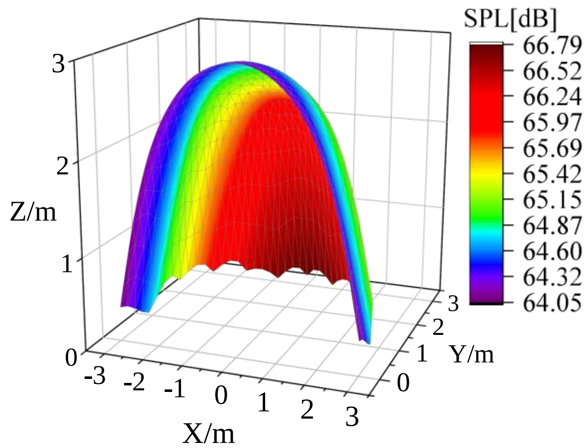

(c) d=3mm.

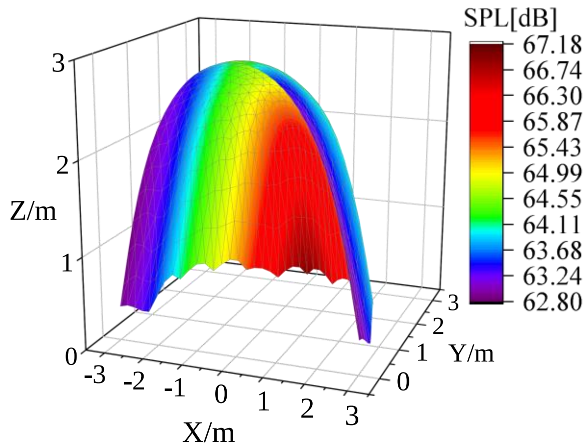

(d) d=4mm.

Fig. 6. Sound field distribution at a wind speed of 15 m/s.

TABLE IV
OVERALL SOUND PRESSURE LEVELS.

d(mm)	Evaluation index	SPL(dB)
	Maximum value	73.46
1	Minimum value	68.42
	Average value	69.25
	Maximum value	64.3
2	Minimum value	59.16
	Average value	61.21
	Maximum value	66.79
3	Minimum value	64.06
	Average value	65.24
	Maximum value	67.17
4	Minimum value	62.8
	Average value	64.48

The medium used in this study is high-speed air, and the resulting noise predominantly manifests as aerodynamic noise, which includes jet noise and turbulence noise. Jet noise is generated by the vigorous mixing of high-speed airflow with stationary air, producing fluctuations in pressure. In contrast, turbulence noise arises from pressure oscillations caused by the formation and collapse of vortices within the flow field [28].

Both noise types are rooted in flow instability. Given the unavoidable presence of turbulence, optimizing radiator design to enhance flow stability holds significant practical value for reducing flow-induced noise.

VI. SPECTRUM ANALYSIS

To further analyze the noise characteristics in an intuitive manner, a quantitative analysis of the sound pressure at the monitoring point within the driver's cab sound field is conducted. Consequently, the next step involves examining the frequency characteristics of the sound source at this monitoring point.

In the flow field, phenomena such as separated flow and vortices induce pressure fluctuations, which are subsequently transformed into sound pressure fluctuations. However, relying solely on the time-domain representation of sound pressure fluctuations makes it challenging to accurately evaluate the intensity of these fluctuations across different frequencies. Thus, it is essential to apply a Fast Fourier Transform (FFT) to the time-domain sound pressure data, converting it into the frequency domain for detailed analysis [29] . To facilitate intuitive comparison, the frequency data is processed logarithmically, and the resulting spectrum of the sound pressure level at a representative monitoring point is illustrated in Figure 7.

The spectrum analysis reveals that all four monitoring points exhibit the following characteristics:

In the frequency range of 20–370 Hz, the sound pressure level decreases as the fin spacing increases.

In the mid-to-high frequency range of 1350–5000 Hz, variations in radiator fin spacing lead to distinct peaks and troughs in the sound pressure level at the monitoring point. Specifically, the sound pressure level for a radiator with a fin spacing of 1 mm consistently fluctuates at a higher magnitude, whereas that with a fin spacing of 2 mm exhibits fluctuations at a lower magnitude.

When comparing conditions across different fin spacings, these findings align with the overall sound field characteristics previously analyzed. Based on this spectrum analysis, an optimal fin spacing exists in the radiator design, where the trade-off between flow resistance and noise generation achieves the best balance.

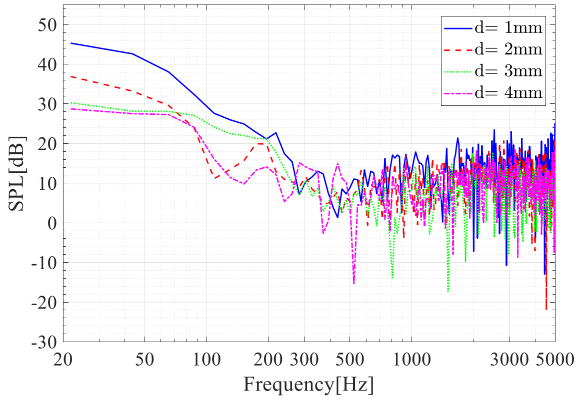

(a) Monitoring point A.

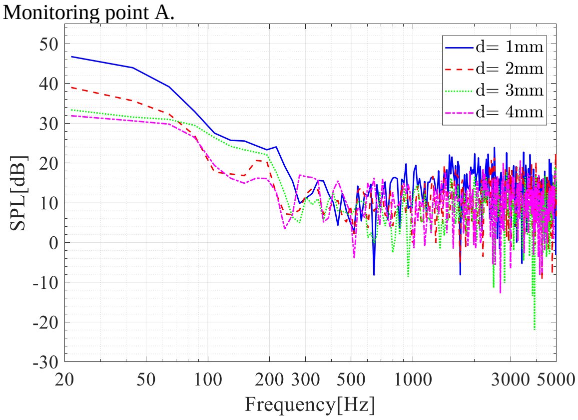

(b) Monitoring point B.

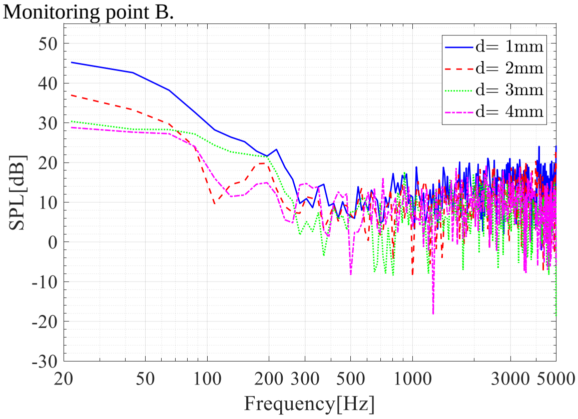

(c) Monitoring point C.

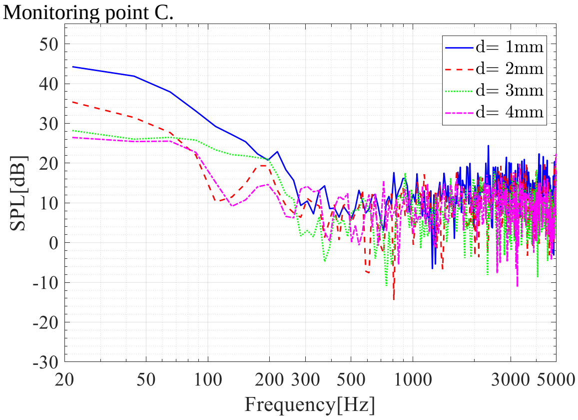

(d) Monitoring point D.

Fig. 7. Sound pressure level spectrum at typical monitoring points.

To quantitatively compare the impact of different radiator noises on the driver's cab, this paper introduces sound quality parameters for comparison and analysis.

The most commonly used objective parameters in psychoacoustics are loudness and sharpness, which intuitively describe the intensity and harshness of in-vehicle noise. The standard unit of loudness, sone, is defined as the perceived intensity reference value of a 1 kHz pure tone at a sound pressure level (SPL) of 40 dB. Its mathematical model is predominantly based on the Zwicker model specified in ISO 532B:

$$N' = 0.08\left(\frac{E_{TQ}}{E_O}\right)^{[(0.5+0.5\frac{E}{E_{TQ}})^{0.23}-1]} \tag{8}$$

where E represents the sound excitation, E_O is the excitation at the absolute hearing threshold, and E_{TQ} is the excitation at the reference sound intensity. By integrating N' over the total Bark scale, the total loudness L_d is obtained:

$$L_d = \int_0^{24\text{Bark}} N'(z)dz \tag{9}$$

The standard unit of sharpness, acum, is defined as the perceived stimulation of a 160 Hz narrowband noise (with a center frequency of 1 kHz and an SPL of 60 dB). Its calculation formula is as follows:

$$S = k \times \frac{\int_0^{24Bark} N'(z) \times g(z)dz}{\int_0^{24Bark} N'(z)dz} \tag{10}$$

where S is the sharpness; the specific loudness N' represents the loudness of the sound within a critical band, reflecting the objective distribution of loudness in the frequency domain; N is the total loudness; k is the weighting coefficient, typically set to 0.1; and $g(z)$ is the weighting function for different critical bands, expressed as:

$$g(z) = \begin{cases} 1 & 16 \le z \le 24 \\ 0.06e^{0.17z} & z < 16 \end{cases} \tag{11}$$

The psychoacoustic parameters were calculated for the spectral data from four monitoring points in the driver's cab direction, and the average loudness and sharpness data were obtained, as shown in Table 5.

From the table, it can be observed that the radiator with a fin spacing of 1 mm exhibits the highest average noise loudness at the monitoring points, measuring 11.83 sone. In contrast, when the fin spacing is 2 mm, the average loudness at the monitoring points in the driver's cab direction is the lowest, indicating that the noise from the radiator at this spacing is perceived as the weakest in the driver's cab, being 38.1% lower than that of the 1 mm radiator.

However, at the same time, the average sharpness at the monitoring points in the driver's cab direction increases as the fin spacing increases. This suggests that as the fin spacing becomes larger, the noise generated by the radiator becomes sharper and more piercing. Specifically, when the fin spacing is 1 mm, the sharpness is the lowest, being 75.6% lower than that of the 4 mm spacing.

TABLE V

PSYCHOACOUSTIC PARAMETERS AT MONITORING POINTS.

d (mm)	Average loudness (sone)	Average sharpness (acum)
1	11.83	2.2
2	7.32	5.93
3	9.52	5.98
4	8.30	9.02

Since the trends of loudness and sharpness are not aligned, a comprehensive noise index P_a is proposed based on loudness and sharpness to more intuitively compare the noise performance of radiators with different fin spacings.

First, loudness and sharpness are subjected to dimensionless processing. As both are negative indicators—meaning that higher values correspond to poorer performance—the range transformation method is applied for normalization:

$$y_i = \frac{\max(x_i) - x_i}{\max(x_i) - \min(x_i)} \tag{12}$$

where x_i and y_i represent the experimental and normalized values of the indicators x , respectively, $\max(x_i)$ and $\min(x_i)$ denote the maximum and minimum values of (N), respectively.

After linear processing, the normalized loudness and sharpness are denoted as P_s and P_c , respectively. By assigning equal weights to loudness and sharpness, the expression for the comprehensive noise index P_a is derived as follows:

$$\mathrm{P_a} = 0.5\ \mathrm{P}_s + 0.5\ \mathrm{P}_c \tag{13}$$

TABLE VI

COMPREHENSIVE NOISE INDEX AT MONITORING POINTS.

d(mm)	P_s	P_c	P_a
1	0	1	0.5
2	1	0.453	0.75
3	0.514	0.446	0.48
4	0.783	0	0.39

Table 6 presents the comprehensive noise index data for monitoring points with different fin spacings. From the table, it is evident that among the four groups of radiators, the one with a fin spacing of 2 mm achieves the highest comprehensive noise index. This indicates that the noise generated by this radiator in the driver's cab direction performs best in terms of both intensity and sharpness compared to the other three groups, showing a 92.3% improvement over the 4 mm radiator, which has the lowest comprehensive noise index.

The comprehensive spectrum analysis and comparison of the comprehensive noise index fully confirm that the optimal fin spacing for the radiator is 2 mm. This finding holds significant engineering application value and provides a critical foundation for the acoustic optimization design of radiators.

VII. CONCLUSIONS

This study investigates the noise characteristics of radiators with different fin spacings through numerical simulation and acoustic analysis. The results indicate the following:

1) Under the operating condition with an inflow velocity of 15 m/s, the radiator with a fin spacing of 2 mm exhibits the smallest high-speed jet region and the best flow characteristics.

2) Under this condition, as the fin spacing increases from 1 mm to 4 mm, the overall noise level of the radiator decreases by approximately 5-9 dB. The maximum noise level drops

from 73.46 dB to 67.17 dB, representing a reduction of 6.29 dB.

3) Under the same condition, the noise distribution trends vary with different fin spacings. At a fin spacing of 1 mm, the high-noise region is highly concentrated in the central area of the radiator, with sound pressure levels ranging between 72–73 dB. In contrast, at a fin spacing of 4 mm, the high-noise region spreads toward both sides, but its magnitude decreases to approximately 64–66 dB.

4) Among the four fin spacing groups, the radiator with a fin spacing of 2 mm generates the lowest noise loudness in the driver's cab direction, achieving a 38.1% reduction compared to the radiator with the highest loudness. Meanwhile, the radiator with a fin spacing of 1 mm produces the lowest noise sharpness in the driver's cab direction, being 75.6% lower than that of the radiator with the highest sharpness.

5) In terms of the comprehensive noise index, the radiator with a fin spacing of 2 mm demonstrates the best overall performance, indicating that the noise it generates in the driver's cab direction outperforms the other three groups in terms of both intensity and sharpness, with a 92.3% improvement over the radiator with the poorest performance.

The findings of this study not only elucidate the complex characteristics of radiator aerodynamic noise and its relationship with fin spacing but also provide a clear direction for further research into the mechanisms of aerodynamic noise generation in radiators. Future studies could focus on exploring the low-noise phenomenon observed at a fin spacing of 2 mm, employing flow field visualization techniques to investigate its underlying mechanisms in depth, and conducting multi-physics coupling analyses. Such in-depth research is expected to facilitate the development of next-generation radiator designs that are more efficient and quieter.

REFERENCES

[1] Zeng Zhixin, Feng Bo, Cui Zhenhua, et al. "Study on aerodynamic noise of radiator fan and improvement of bionics ," Mechanical Science and Technology for Aerospace Engineering, 2022, 41(06): 954-960.

[2] Zarri A, Christophe J, Moreau S, et al. "Influence of swept blades on low-order acoustic prediction for axial fans," Acoustics. MDPI, 2020, 2(4): 812-832.

[3] Liu Gang, Wang Lei, Liu Xiaomin. "Numerical investigation on effects of blade tip winglet on aerodynamic and aeroacoustic performances of axial flow fan," Journal of Xi'an Jiaotong University, 2020, 54(07): 104-112.

[4] Wang Menghao, Wu Liming, Liu Xiaomin, et al. "A study on noise reduction of centrifugal fan in air conditioner by using the bionic blade inspired by the owl wing," Journal of Xi'an Jiaotong University, 2018, 52(06): 55-61.

[5] Liu Xiaomin, Li Shuo. "Effects of bionic volute tongue bioinspired by leading edge of owl wing on aerodynamic performance and noise of multi-blade centrifugal fan," Journal of Xi'an Jiaotong University, 2015, 49(01): 14-20+33.

[6] Huang Yi, Long Shucheng, Li Zhi, et al. "Numerical simulation prediction and analysis of aerodynamic noise of engine cooling fans," Noise and Vibration Control, 2021, 41(06): 173-178.

[7] Dong Yueqianxun, Guo Hao, Wang Shuwen. "Bionic design and noise reduction analysis of automobile cooling fan blades," Noise and Vibration Control, 2022, 42(04): 196-200.

[8] Luo Laibin, Wu Yadong,Ouyang Hua. "Experimental and numerical study on the noise of Uneven-spaced automobile cooling fans," Noise and Vibration Control, 2021, 41(05): 175-181.

[9] Tang Jie, Zhu Maotao. "Research on noise reduction of vehicle cooling fan with sawtooth structure," Journal of Chongqing University of Technology(Natural science), 2022, 36(10): 100-110.

[10] Rydlewicz W, Rydlewicz M, Pałczyński T. "Experimental investigation of the influence of an orifice plate on the pressure pulsation amplitude in the pulsating flow in a straight pipe," Mechanical Systems and Signal Processing, 2019, 117: 634-652.

[11] Xie Hui, Ge Xiyun, Liu Jian, Liu Shuai. "Throttling and acoustic characteristics of throttling orifice plate with different configurations," Journal of Northeastern University(Natural Science), 2020, 41(04): 587-593.

[12] Wang Y, Liu T, Sha J, et al. "Large eddy simulation-based analysis of the flow-induced noise characteristics of shell and tube heat exchanger," International Communications in Heat and Mass Transfer, 2023, 148: 107030.

[13] Bi J, Liu J, Jiang Y. "Signal-to-noise research on comprehensive performance of plate heat exchanger for commercial electric vehicle," International Journal of Thermal Sciences, 2021, 165: 106967.

[14] Rynell A, Efraimsson G, Chevalier M, et al. "Acoustic characteristics of a heavy duty vehicle cooling module," Applied Acoustics, 2016, 111: 67-76.

[15] Hu D, Dong W, Gao P, et al. "Noise reduction optimization for numerous radiator fans for fuel cell vehicle considering thermal-fluid-acoustic synergy," International Journal of Heat and Mass Transfer, 2024, 223: 125231.

[16] Han T, Wang L, Cen K, et al. "Flow-induced noise analysis for natural gas manifolds using LES and FW-H hybrid method," Applied Acoustics, 2020, 159: 107101.

[17] Zarri A, Botana M B, Christophe J, et al. "Aerodynamic investigation of the turbulent flow past a louvered-fin-and-tube automotive heat exchanger," Experimental Thermal and Fluid Science, 2024, 155: 111182.

[18] Czwielong F, Soldat J, Becker S. "On the interactions of the induced flow field of heat exchangers with axial fans," Experimental Thermal and Fluid Science, 2022, 139: 110697.

[19] Amoiridis O, Zarri A, Zamponi R, et al. "Sound localization and quantification analysis of an automotive engine cooling module," Journal of Sound and Vibration, 2022, 517: 116534.

[20] Sanjosé M, Moreau S. "Fast and accurate analytical modeling of broadband noise for a low-speed fan," The Journal of the Acoustical Society of America, 2018, 143(5): 3103-3113.

[21] Wang Dong, Zhang Xueliang, Li Qi. "Numerical simulation on aerodynamic noise of helmholtz resonator," Computer Aided Engineering, 2012, 21(6): 5-10.

[22] Li Qian, Ji Hua, Feng Donglin, et al. "Effects of hole distribution on flow field and noise for multi-hole plates," The Chinese Journal of Process Engineering, 2022, 22(05): 601-611.

[23] Zhu Penghui, Jiang Jinhui, Cui Wenxu. "Analysis of rotor vibration response and noise based on two-way fluid-structure coupling," Journal of Nanjing University of Aeronautics & Astronautics, 2024, 56(02): 242-252.

[24] Ma Ying, Duan Qingjuan, Hu Ruifeng, et al. "Numerical simulation and flow calibration of multi-hole orifice and wedge throttle devices," Journal of Xidian University, 2018, 45(1): 60-65.

[25] Kim M, Lee H, Hwang W. "Experimental study on the flow interaction between two synthetic jets emanating from a dual round orifice," Experimental Thermal and Fluid Dcience, 2021, 126: 110400.

[26] Paruchuri C, Subramanian N, Joseph P, et al. Broadband noise reduction through leading edge serrations on realistic aerofoils[C]//21st AIAA/CEAS aeroacoustics conference. 2015: 2202.

[27] Asghar A, Perez R E, Jansen P W, et al. Application of leading-edge tubercles to enhance propeller performance[J]. AIAA Journal, 2020, 58(11): 4659-4671.

[28] Ouyang Zhixiong, Zhang Wenqing. "Study on flow and noise characteristics of valve sleeve holes in steam valves," Modeling and Simulation, 2022, 11: 916..

[29] Mo Xueping, Shao Jiaru, Zheng Zijun, et al. "Aerodynamic noise characteristics of serrated structure airfoil in adverse pressure gradient," Flight Dynamics, 2023, 41(03): 13-19+39.

Jie Meng, male. The author is an Associate Professor at Taiyuan University of Science and Technology. Meng was born in China. In 2018, he received his PhD in Mechanical Engineering from Taiyuan University of Science and Technology, Shanxi Province, China. Mainly research topics: mechanical system dynamics analysis, mechanical structure design and optimization, and bionic mechanical research and application.

As an ASSOCIATE PROFESSOR, he is currently working at the School of Vehicle and Transportation Engineering, Taiyuan University of Science and Technology.

Selected publications:

(1) Jie Meng, Dagang Sun. "Research on Vibration Suppression of Wind Turbine Blade Based on Bamboo Wall Three-layer Damping Structure" Journal of Vibroengineering, 2017, vol. 19, pp. 87-99. (SCI)

(2) Jie Meng, Dagang Sun. “Structural Optimization of Wind Turbine Blades with Ring Shear Webs” Journal of the Brazilian Society of Mechanical Sciences and Engineering, 2018, vol. 40, no. 313. (SCI)
(3) Jie Meng, Yongxiang Mu, Xiaochang Ma. “Analysis on the Vibration Performance of Spruce Structure with Variable Cross-Section Under Snow Load by Semi-Analytical Method” International Journal of Structural Stabilityand Dynamics, 2023. (SCI)
His research interests:
Key technologies of large wind turbine blade dynamics and vibration suppression, vehicle chassis dynamics and structure optimization, bionic damping structure design, and vibration and noise reduction technology.